616 J. Med. Chem. 2010, 53, 616–623
DOI: 10.1021/jm9010669

Journal of Medicinal Chemistry Article

A Novel Potent Nicotinamide Phosphoribosyltransferase Inhibitor Synthesized via Click Chemistry

Giampiero Colombano,[§,†] Cristina Travelli,[§,†] Ubaldina Galli,[†] Antonio Caldarelli,[†] Maria Giovanna Chini,[‡] Pier Luigi Canonico,[†] Giovanni Sorba,[†] Giuseppe Bifulco,[‡] Gian Cesare Tron,*[,†] and Armando A. Genazzani[†]

[†]*Dipartimento di Scienze Chimiche, Alimentari, Farmaceutiche e Farmacologiche, Università degli Studi del Piemonte Orientale A. Avogadro, Via Bovio 6, 28100 Novara, Italy and* [‡]*Dipartimento di Scienze Farmaceutiche, Università di Salerno, Via Ponte Don Melillo, 84084 Fisciano (SA), Italy.* [§]*These authors contributed equally to the present work.*

Received July 19, 2009

The inhibition of NAD synthesis or salvage pathways has been proposed as a novel target for antitumoral drugs. Two molecules with this mechanism of action are at present undergoing clinical trials. In searching for similar novel molecules, we exploited copper-catalyzed [3 + 2] cycloaddition between azides and alkynes (click chemistry) to synthesize 185 novel analogues. The most promising compound displays an IC_{50} for cytotoxicity in vitro of 3.8 ± 0.3 nM and an IC_{50} for NAD depletion of 3.0 ± 0.4 nM. Herein, we strengthen previous data suggesting that this class of compounds induces autophagic cell death. In addition to characterizing this compound and providing a rationale via molecular docking, we reinforce the excellent potential of click chemistry for rapidly generating structure−activity relationships and for drug screening.

Introduction

While the pharmacological fight against cancer has made great advances in the last 20 years, novel molecules to fight this disease are still urgently needed. Many cancers still present unmet therapeutic needs, and chemoresistance is an important phenomenon within the context of fast cell division and high mutation rates. Furthermore, side effects and safety are major concerns with antitumoral drugs. Although targeted biotechnology-based agents (e.g., monoclonal antibodies and vaccines) have and are being developed for a number of cancers, it is obvious that small-molecule drugs will result in lower costs and might be able to combat a wider range of tumors. Furthermore, the development of novel agents might also allow researchers to discover synergisms that will reduce the doses required for single agents used in combination, increasing efficacy while reducing side effects. For this to occur, it is imperative that novel targets be exploited and that, for each target, a number of therapeutic agents (for example, with different pharmacokinetic profiles or different organotropisms) become available to the clinician.

In this context, it has recently been proposed that interfering with NAD(P) levels might lead to cell death of those cells that have a high usage rate of this pyridine nucleotide, that is, tumoral cells with a high division rate.[1] While the general perception is that NAD(P) is mainly used as an enzymatic cofactor (and, as such, its depletion should be slow as it participates mainly in redox reactions), it is now accepted that a number of enzymes consume NAD(P). For example, NAD is the substrate for a specific subclass of histone deacetylases (sirtuins),[2−4] as well as mono- and poly-ADP ribosylating enzymes (e.g., PARPs[a]).[3,4] Furthermore, NAD(P) is also the precursor for a number of Ca^{2+}-releasing second messengers (e.g., cADPR, NAADP) and as such is consumed by enzymes such as CD38.[5,6]

Eukaryotic cells possess several mechanisms to replenish NAD levels, including a *de novo* pathway from tryptophan and at least two salvage/recycling pathways.[7,8] The most important of these latter two pathways relies on the enzyme nicotinamide phosphoribosyltransferase (NMPRTase), which converts nicotinamide into nicotinamide mononucleotide (NMN), which is subsequently converted to NAD by NMN adenyltransferase (NMNAT).

NMPRTase has been exploited as a target for developing a potential antitumoral drug (**1**, initially known as FK866 and now renamed APO866).[9] This compound has an IC_{50} for cytotoxicity of approximately 1 nM against several cancer cell lines, and when evaluated preclinically it has been demonstrated to possess very promising antitumoral actions against both solid tumors and leukemia cells.[9,10] Phase I clinical trials have been completed, and this compound is at present in phase II alone or in combination with other antitumoral drugs.[11] A second compound, **2** (CHS 828, now renamed GMX1777) (Figure 1), is in early clinical development.[12] This compound, originally screened as an antihypertensive drug,[13] showed very high cytotoxic activity.[14] Furthermore, its action, as for **1**, can be reverted by adding nicotinamide, the true substrate for NMPRTase.[9,14]

We recently attempted to replace the amide of **1** with a 1,4-disubstituted triazole using click chemistry, as it has been postulated that this substitution can generate a nonclassic bioisostere.[15] To our surprise, the true bioisostere (**3**) was

*To whom correspondence should be addressed: tel, +39-0321-375857; fax, +39-0321-375821; e-mail, tron@pharm.unipmn.it.

[a] Abbreviations: PARPs, poly-ADP-ribose polymerases; cADPR, cyclic adenosine diphosphoribose; NAADP, nicotinic acid adenine dinucleotide phosphate; NMPRTase, nicotinamide phosphoribosyl transferase; NMN, nicotinamide mononucleotide; NMNAT, nicotinamide mononucleotide adenylyltransferase; MTT, 3-(4,5-dimethylthiazol-2-yl)-2,5-diphenyltetrazolium bromide; LC3, microtubule-associated protein 1A/1B light chain 3; EGFP-LC3, enhanced green fluorescent protein−microtubule-associated protein 1A/1B light chain 3.

 Published on Web 12/04/2009

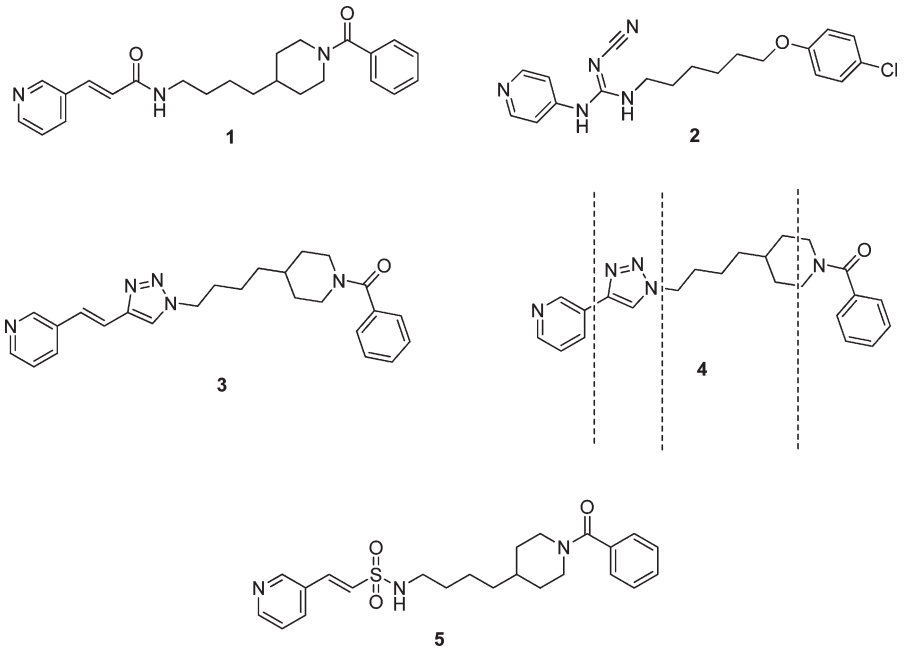

Figure 1. NMPRTase inhibitors in clinical trials (**1** and **2**) and analogues of FK866 used to draw the original hypothesis (**3**, **4**, and **5**).

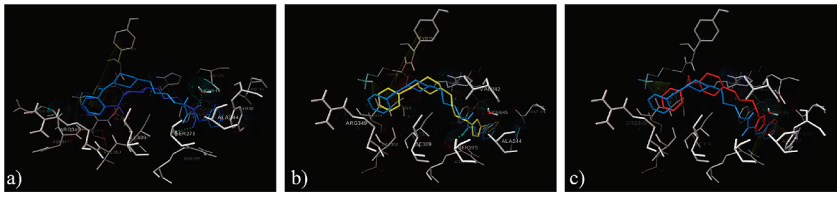

Figure 2. Superimposition of the crystallized **1** structure[16] and the structures calculated by molecular docking in the catalytic site of NMPRTase. The true crystallized **1** structure is present in all panels (light blue), superimposed with the calculated **1** (a, blue), the calculated **3** (b, yellow), and the calculated **4** (c, red). The NMPRTase A and B chains are represented by gray sticks. The figure highlights $\pi-\pi$ stacking, cation$-\pi$, hydrophobic interactions, and hydrogen bonds of the target$-$ligand complex.

devoid of activity up to micromolar concentrations, while the triazolyl pyridine derivative (**4**) maintained nanomolar potency even while being approximately 80-fold less potent than **1**. This observation suggests that the 1,4-disubstituted triazole ring is compatible with the binding pocket of the enzyme (Figure 1). We then performed molecular docking calculations on nicotinamide phosphoribosyltransferase (NMPRTase) and **1**, **3**, and **4**. Tong et al. in 2006 elucidated the X-ray crystal structure of the human NMPRTase$-$**1** complex (PDB code: 2GVJ) with a 2.1 Å resolution.[16] The authors clarified the molecular mechanism for the substrate specificity of this enzyme, defining the binding mode of **1** and the structural basis for its specificity for NMPRTase. The structure revealed a tunnel at the interface between chains A and B that is a potential binding site for inhibitors. The first step of our molecular docking studies was the validation of the docking method. In accordance with that reported by Tong et al.,[16] we left water molecule 645 in the NMPRTase active site during the molecular docking calculations with Autodock3.0.5 software.[17] Moreover, to improve the accuracy of calculated dissociation constant (K_{dcalcd}), we performed energy and geometry optimizations of **1**, **3**, and **4** and computed the charges of the molecules at the quantum mechanical (QM) level (see computational details).

In analogy with the rationalization of the NMPRTase inhibitor pharmacophore elucidated by Tong et al.,[16] our calculated model for **1** maintains all of the principal interactions with the enzyme: (1) the pyridine ring of the inhibitor is sandwiched between the side chains of Phe193 and Tyr18′, and it forms a cation$-\pi$ with Arg196; (2) the carbonyl oxygen atom and the amide nitrogen of the amide bond form two hydrogen bonds with the hydroxyl of Ser275 and the water molecule, respectively. Moreover, the lead compound establishes hydrophobic interactions with the amino acids of the tunnel formed at the dimer interface, namely, Glu376, Asn377, Arg349, Ile378, Val330, Val350, Ala379, Ile351, and Ile309. In particular, the phenyl ring forms a π-stacking interaction with Tyr188 on the shallow groove of the NMPRTase surface. All of the above-mentioned interactions (Figure 2a) contribute to the **1**$-$enzyme complex calculated stability ($K_{dcalcd} = 1.23 \times 10^{-9}$ M) and strengthen our model. Analyses of other compounds were conducted by taking into account the similarities and/or differences with the binding mode of **1**. The 1,4-disubstituted triazole rings of compounds **3** and **4** are able to form a hydrogen bond with the OH of Ser275 but cannot form it with the water molecule; this is a drawback that may be associated with the lower activities of both **3** and **4** with respect to the lead compound.

The difference in activity between the true bioisostere (**3**) and the triazolyl pyridine derivative (**4**) is due to the different topological position of the pyridine ring (Figure 2b). The presence of the double bond between the triazole and pyridine ring causes the loss of $\pi-\pi$ stacking with Phe193 and Tyr18′, suggesting decreased activity. On the other hand, **4** has the

same topological position of the pharmacophoric points of **1** cocrystallized with the enzyme (Figure 2c), and moreover the phenyl ring forms a cation$-\pi$ interaction with Lys189 on the NMPRTase surface ($K_{dcalcd} = 1.89 \times 10^{-9}$ M).

In a set of unpublished data, we also synthesized a compound bearing a sulfonamide group (**5**) in place of the amide moiety of **1** (Figure 1). The sulfonamide should theoretically be more prone to form a hydrogen bond due to its higher acidity. Yet, this compound (either for inability of the drug to cross the plasma membrane or inability to enter the binding pocket) was inactive (see Supporting Information).

This failure led us to exploit the compatibility of the triazolyl pyridine with the active site of NMPRTase to explore the possibility of generating more active analogues. Indeed, the triazolyl pyridine also presents the great advantage of allowing us to capitalize on the simplicity of the click chemistry reaction.[18,19] Its amenability to solution phase parallel synthesis is also an advantage, as it allows the screening of a high number of analogues in a fast and reliable manner.[20−22] This, in turn, allows probing of the active site and the rim of the enzyme in more detail.

We now report the synthesis of 185 triazolyl pyridines, using a fast and versatile solution-phase parallel combinatorial synthesis via click chemistry. The most promising of these compounds displays an IC_{50} for cytotoxicity in vitro of 3.8 ± 0.3 nM and an IC_{50} for NAD depletion of 3.0 ± 0.4 nM.

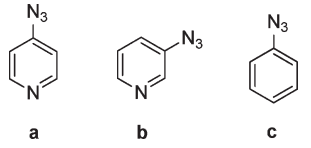

Figure 3. Synthesized aromatic azides used to generate the first library.

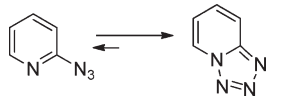

Figure 4. Predominant tetrazolic form of 2-azidopyridine.

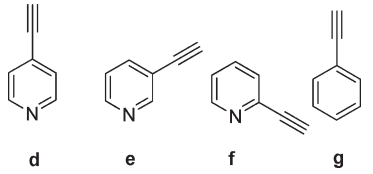

Figure 5. Aromatic alkynes used.

Chemistry

To generate novel NMPRTase inhibitors, we rationalized the structure of the lead compound (**4**) and subdivided it in four domains: the aromatic ring, the triazole ring, the alkyl chain, and the hydrophobic tail (Figure 1). We then proceeded to synthesize the building blocks. The archetypical click chemistry is a two-component reaction in which an alkyne and an azide react in the presence of copper(I) salts to give rise to a 1,4-disubstituted 1,2,3-triazole. We therefore decided to generate building blocks bearing the aromatic ring (pyridine or phenyl) and building blocks containing an alkyl chain with a hydrophobic tail. We generated compounds bearing the triazole in both orientations (i.e., functionalizing the aromatic ring with either the azide or the alkyne group).

For the aromatic rings bearing the azide group, we prepared 4- and 3-azidopyridine (**a** and **b**) and phenyl azide (**c**). Compounds **b** and **c** were prepared using classical diazotation−azidation protocols,[20] while **a** was prepared via aromatic nucleophilic substitution of 4-chloropyridine with sodium azide[23] (Figure 3).

2-Azidopyridine was not used as it is well-known that it predominantly exists in its tetrazolic form[24] and failed to react with alkynes in copper-catalyzed [3 + 2] azide−alkyne cycloaddition (Figure 4).

For the aromatic rings bearing the alkyne group, we used 4-, 3-, and 2-ethynylpyridine (**d, e**, and **f**, respectively) and phenylacetylene (**g**) (Figure 5). Compound **d** was synthesized using Bestmann−Ohira reagent,[25,26] starting from 4-pyridine carboxaldehyde, while **e**, **f**, and **g** were commercially available.

For the alkyl chain with the hydrophobic tail, we purchased seven commercially available hydrophobic alkynes (**A**−**G**) (Figure 6). These were coupled with the azides **a**−**c** previously prepared.

We then prepared 10 hydrophobic azides (**H**−**K**) (Figure 7) and reacted them with alkynes **d**−**g** to generate a first library of 61 members.

Subsequently, a second library was prepared starting from three different ω-bromoalkyl carboxylic acids. The azides were prepared by reacting sodium azide and the bromides of choice in DMF in quantitative yields. The carboxylic acids were then activated as acyl chlorides and then coupled with 10 different hydrophobic amines to give the desired building blocks (**L**−**U**) (Scheme 1, Figure 8). These compounds were directly coupled with alkynes **d**−**g**, without further purification. The building blocks described above were used to synthesize 120 compounds in parallel fashion.

The final products were either obtained by precipitation from the reaction mixture (100/185; yields 50−90%; purity > 80% on average) or by evaporation of the solvent

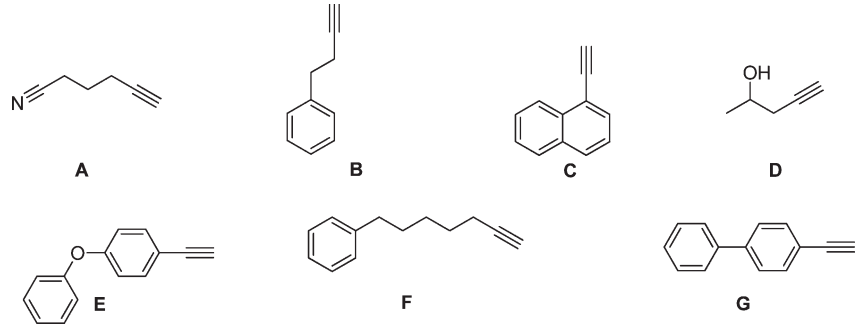

Figure 6. Commercially available alkynes used to generate the first library.

and used as such in the preliminary screening. This approach has the advantage of simplicity and speed but might lead to both false positives and negatives. For example, copper will be present in the samples obtained by evaporation. In order to rule out its potential undesired effect, we tested different copper salts at the highest expected concentration. As a result, the viability of the cells was not compromised (data not shown). In support of this approach, it should be noted that our laboratory and others have used this preliminary evaluation previously without observing false positives.[22] As triazole may chelate copper, it cannot be excluded that the formation of the complex may lead to false negative results. Yet, it could be expected that if this were to occur, all the triazoyl pyridines should show no activity, and this was not the case.[22]

Biological Evaluation

To investigate the activity of the synthesized compounds, we decided to exploit a neuroblastoma cell line that had already been characterized by us as sensitive to **1**.[15] In brief, we used SH-SY5Y cells and incubated these with a fixed concentration of compound (1 μM) for 48 h. Cell viability was evaluated by the MTT method (and, in parallel, by cell count to confirm the data). Thirteen out of 185 compounds were active (decrease of viability of at least 60%). Some of these compounds were obtained by precipitation and others by evaporation, suggesting that copper salts (present at high concentrations only in the latter) were not responsible for this effect. We then resynthesized the active compounds and purified them by column chromatography. The purity of these compounds (> 95%) was analyzed via elemental analysis and was within ±0.4% of the calculated value unless otherwise noted. We then further characterized these compounds by using the purified samples.

Only one compound (**6**) from the first library was found to have an effect on cell viability (see Supporting Information, Table S1). From the second library, we found that 12 compounds had an effect on cytotoxicity (Supporting Information, Table S2). Promisingly, all of the 12 compounds contained a meta-substituted pyridine, and four different hydrophobic scaffolds were identified (Figure 9). Full concentration response curves were generated, and most compounds were found to have IC_{50} values in the nanomolar range (Table 1, Figure 10). As the 12 compounds from the second library could be grouped by hydrophobic replacement and subdivided by chain length, we also probed their structure−activity relationship. As can be observed in Figure 10a, biphenyl ≫ 1,1′-diphenyl ether > 1,1′-biphenylmethane ≥ 1,1′-diphenylethane.

Scheme 1. Synthetic Scheme for the Preparation of 30 Azides

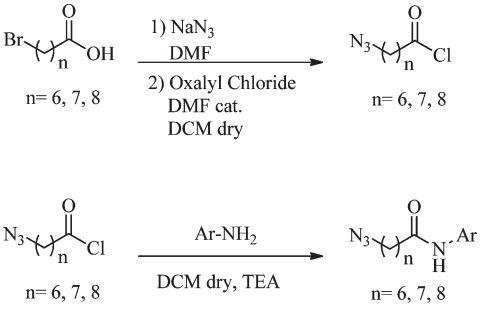

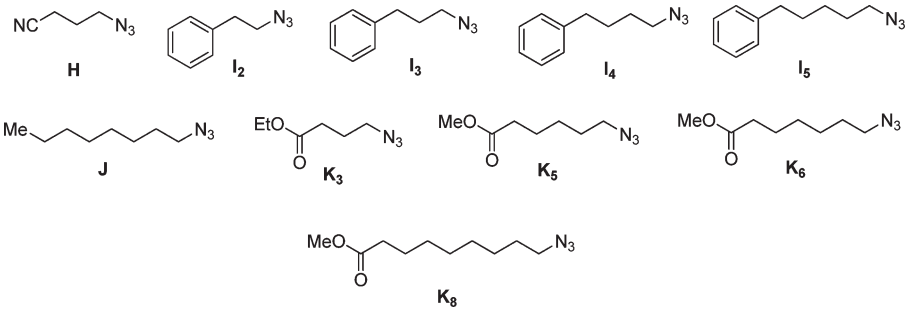

Figure 7. Synthesized azides used to generate the first library.

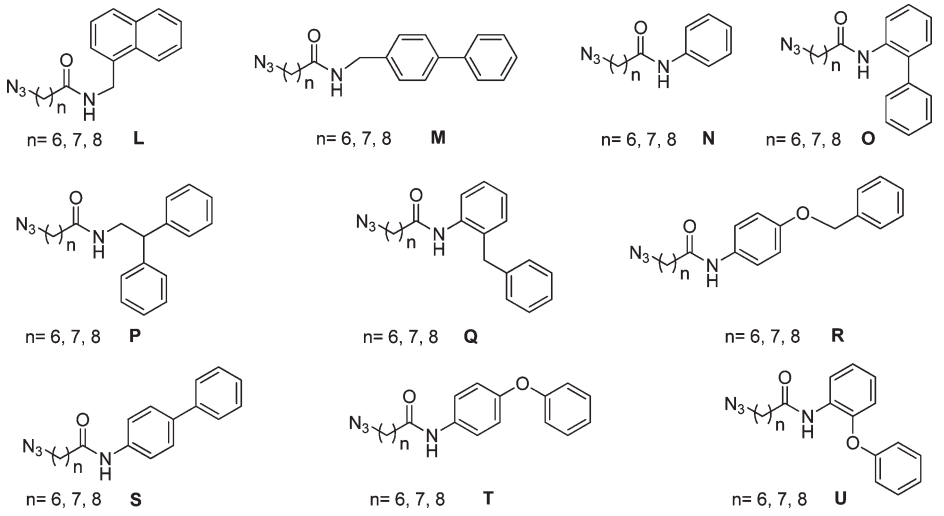

Figure 8. Azides synthesized starting from three different ω-bromoalkyl carboxylic acids.

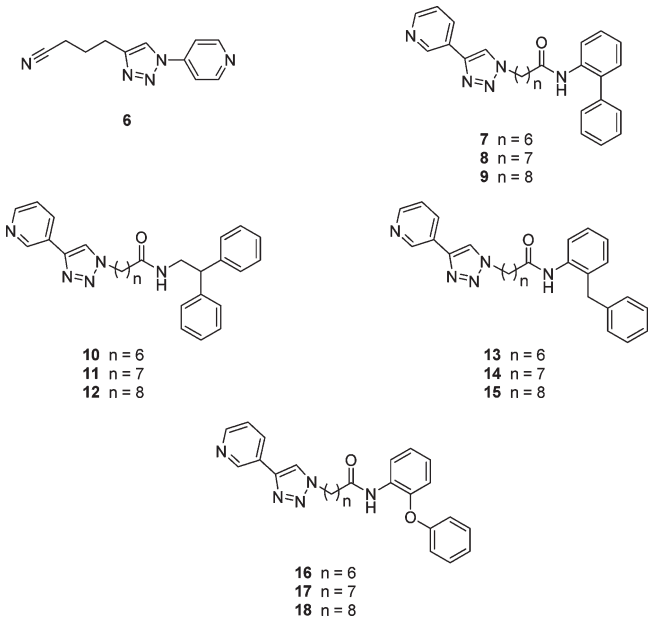

Figure 9. Compounds that emerged from the screening as cytotoxic at 1 μM.

Table 1. Synoptic Biological Data of the Active Compounds That Emerged from the Screening[a]

		NAD levels (% of control)		
compd	viability (IC_{50}, nM)	at 1 μM	at 300 nM	IC_{50}
1	1.7 ± 0.2			0.5 ± 0.1
4	92.9 ± 25.8[b]			5.7 ± 1.3[b]
6	nd[c]	31.0 ± 13.2	87.8 ± 4.6	
7	56 ± 13	26.2 ± 12.0	88.2 ± 2.8	
8	3.8 ± 0.3	11.6 ± 6.2	9.9 ± 7.1	3.0 ± 0.4
9	14.6 ± 3.6	13.0 ± 6.2	35.6 ± 16.7	84.4 ± 6.7
10	nd	16.8 ± 6.9	83.8 ± 2.0	
11	97 ± 17	23.0 ± 9.5	11.0 ± 5.6	49.2 ± 1.8
12	157 ± 50	32.3 ± 6.5	77.3 ± 14.4	
13	nd	28.0 ± 7.6	86.1 ± 6.2	
14	72 ± 12	30.0 ± 9.7	75.2 ± 5.3	
15	82 ± 8	13.1 ± 7.0	74.7 ± 7.3	
16	120 ± 25	24.7 ± 6.0	81.3 ± 4.6	
17	37 ± 7	17.7 ± 8.7	87.9 ± 1.4	
18	78 ± 9	22.6 ± 8.6	79.5 ± 5.9	
19	nd		74.7 ± 7.3	
20	37.4 ± 17.5		12 ± 8.0	17.1 ± 0.1
21	nd		87.9 ± 1.4	
22	205 ± 17.6		79.5 ± 5.9	

[a] Viability was evaluated via the MTT method. Values are mean ± SEM of 8−12 determinations. NAD levels were first screened at a fixed concentration (n = 10), and if the compound displayed significant activity at 300 nM, a full concentration response was performed. Values are mean ± SEM. For cytotoxicity data of the other compounds, see Table S1 (Supporting Information). [b] Data taken from Galli et al.[15] [c] nd: not determined as full cytotoxicity was not reached at concentrations up to 1 μM.

This rank order of potency was also conserved in the other series. Likewise, when probing for side chains (n = 7−9), all of the four series displayed the following rank order of potency: $n = 8 > n = 9 > n = 7$ (Figure 10b). The most potent compound (**8**) was also sent for characterization of cell line specificity at the National Cancer Institute. The results are illustrated in the Supporting Information (Table S3). Compound **8** inhibited the growth of most cell lines tested, with nanomolar potency (GI_{50}) in cell lines derived from leukemia, lung, CNS, colon, melanoma, ovarian, renal, and prostate cancers. To our surprise, this compound appeared truly cytotoxic in melanoma cell lines, while in the others it was mainly cytostatic. This might suggest potential areas of therapeutic use.

Compound **8** was also further modified to gather additional structural information. In this context, we synthesized the ester (**19**) as a possible bioisostere of the amide group, the carbazole (**20**), to rigidify the 2-aminobiphenyl scaffold, and we substituted the phenyl ring at the 2-position of aniline (**21**, **22**) with commercially available ortho-substituted anilines (Figure 11) to explore the role of the *o*-phenyl. Compound **20** (the rigidified analogue) displayed nanomolar potency (37.4 ± 17 nM), albeit with a loss of potency of approximately 10-fold compared to **8.** Compound **22** displayed a decrease of approximately 50-fold (Table 1). Compound **19** did not display any activity. Yet, no conclusion can be drawn for this lack of efficacy as it may be also due to instability of the ester in the medium.

We next set out to investigate whether these compounds induced NAD depletion. As expected, **1** depleted the cellular NAD pool with an IC_{50} of approximately 1 nM. Similarly, compound **8**, compound **20** (the rigidified analogue), and compounds **11** and **9** also depleted NAD pools with the expected rank order of potency (Table 1, Figure 12). To our surprise, the 1,1′-diphenylmethane and 1,1′-diphenyl ether series were devoid of activity on NAD depletion at concentrations below 1 μM, opening the question as to whether their cytotoxicity is correlated to NAD depletion (Table 1). As all of these compounds maintain the pyridine ring, it cannot be excluded that these compounds act also on NAD-using enzymes or deplete selected NAD pools in cells (e.g., mitochondrial). We previously reported that inhibition of NMPRTase can be reverted by extracellular NAD but cannot be reverted by nicotinamide (as the former is downstream of the enzyme while the latter is its substrate).[27] To confirm the mechanism of action of **8**, we coincubated this compound in the presence of either NAD or nicotinamide. As expected, **8** reduced viability (24 ± 3.0% of control), and this effect was reverted by NAD (97 ± 6%) but not by nicotinamide (31 ± 4%).

While initial reports suggested that **1**-induced cell death proceeded by apoptosis,[9] more detailed evaluation of the phenomenon suggests that autophagy might also play an important part both in solid (i.e., neuroblastoma) and in liquid tumors.[10,27,28] Autophagy is a process in which the cell degrades its own components via the lysosomal compartment. This process may function as a protective mechanism in starved cells but also has the capacity to lead to cell death.[29] It would therefore appear reasonable that such a mechanism would be involved in NAD depletion. In other words, NAD depletion (an early event) leads to autophagy as an attempt to survive, and this is then followed by cell death. As this aspect of cancer biology might play an important part in the development of novel analogues to be brought forward to the clinical trials, we decided to assess whether **8** shared these features.

To investigate autophagy, we capitalized on the coupling of the LC3 protein with phosphatidylethanolamine during autophagy,[30] which leads to a protein that runs faster on SDS−PAGE gels. When neuroblastoma cells were treated with either **1** or **8** for 40 h, a second band (known as LC3-II and representing the phosphatidylethanolamine coupled LC3) was observable (Figure 13). It is interesting to note that the band was not observable at earlier time points, when NAD

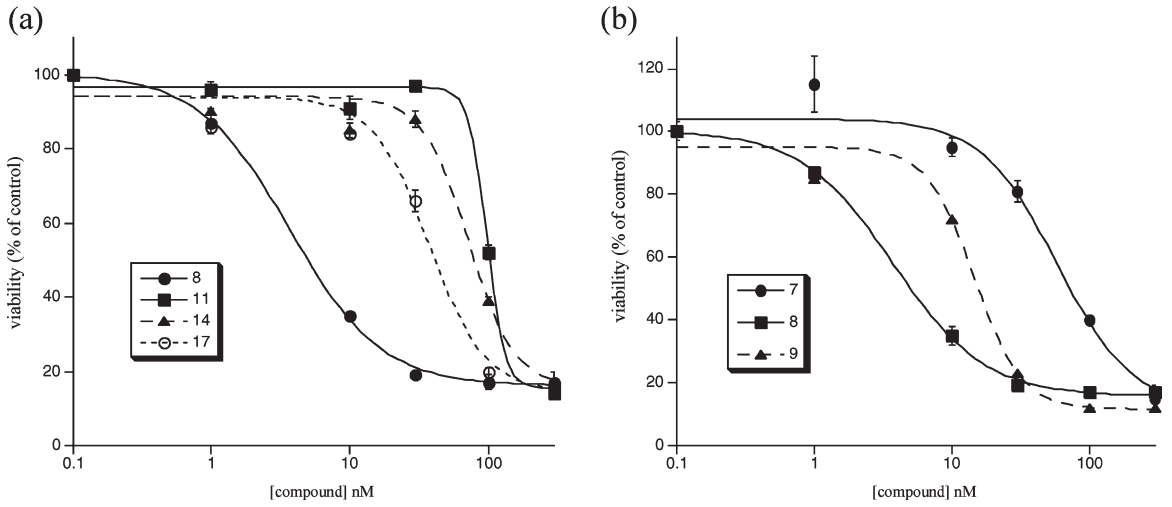

Figure 10. Concentration response curve for cytotoxicity of the compounds that emerged as cytotoxic from the screening. (a) Relative rank order of potency of the four aromatic scaffolds identified as active. All of the compounds depicted had chain lengths of seven carbons. Identical rank order of potency was obtained with the other two series. (b) Relative rank order of potency of the three chain lengths tested. The three compounds had identical aromatic scaffolds. Identical rank order of potency was obtained with the other three series. Values are mean ± SEM of 8−12 determinations.

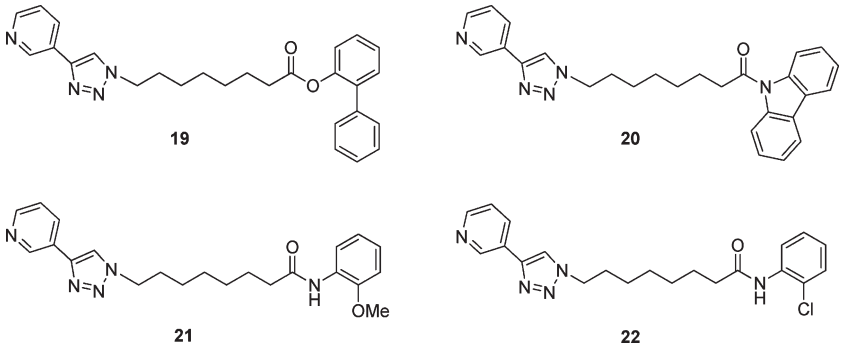

Figure 11. Synthesized analogues of compound **8**.

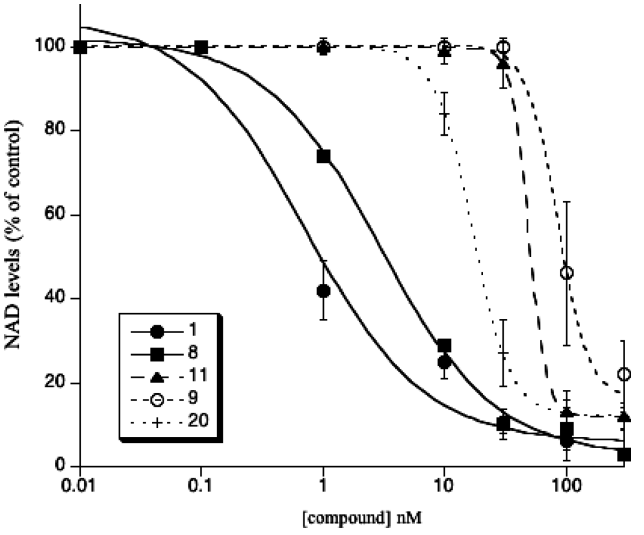

Figure 12. Concentration response curve for NAD depletion of compounds that reduced NAD levels significantly at 300 nM. Values are mean ± SEM of 10−20 determinations.

depletion was already measurable. Unlike LC3-I (which is cytosolic), LC3-II is membrane-bound and is present in autophagosomes. We then transfected cells with EGFP-LC3

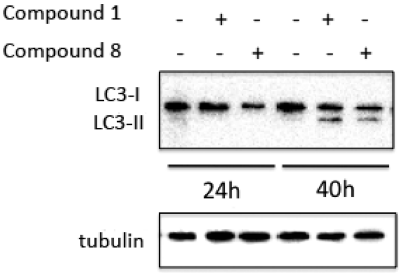

Figure 13. Western blot analysis of LC3-I/II and tubulin in control and treated cells. Compounds **1** and **8** were used at a concentration of 10 nM. The Western blot is representative of six experiments that yielded similar results using two antibodies from different sources.

in order to visualize the cellular localization of LC3-I or -II. As expected, punctate staining of LC3-II and the formation of autophagolysosomes (Figure 14 and insets) were observable when cells were incubated with **8**. Identical results were observed in stably expressing cell lines (Travelli and Genazzani, unpublished). The present data would therefore strengthen the similarity in mechanism of action of **8** and **1**.

Molecular Docking Studies

We then performed molecular docking studies on the compounds with nanomolar potency, **8** and its rigid analogue **20**, using the model described in the Introduction.

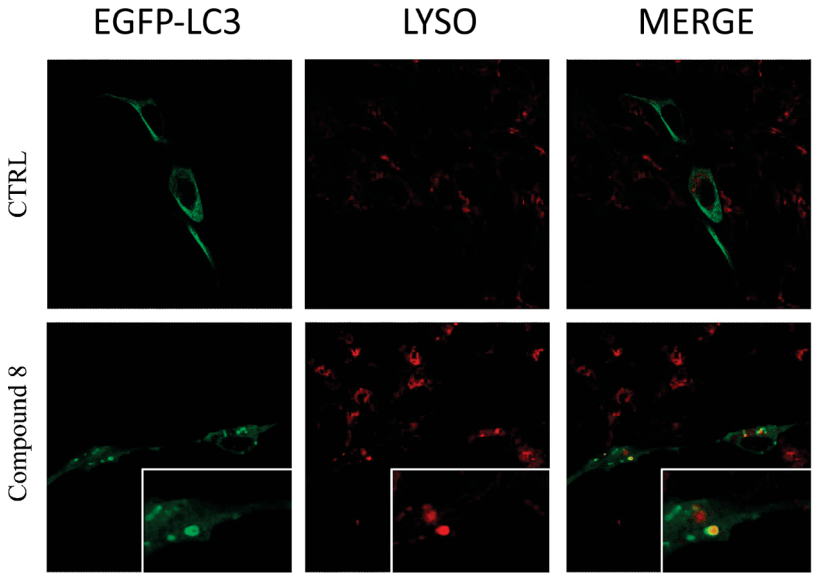

Figure 14. Representative confocal images of EGFP-LC3-expressing SH-SY5Y cells treated with compound **8** (10 nM). LC3 is expressed in green, and lysotracker is expressed in red. The insets represent enlargements showing the formation of autophagic vacuoles. Similar results were observable in stably expressing EGFP-LC3 cells (Travelli and Genazzani, unpublished).

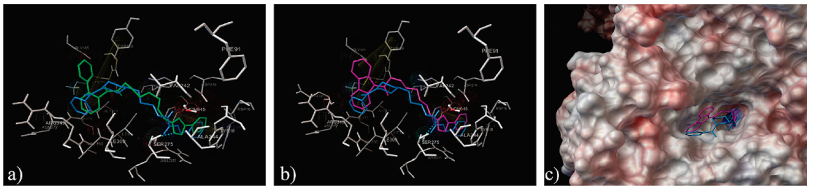

Figure 15. Three-dimensional model of the superimposition in the catalytic site between the true crystallized **1** structure and the calculated structures for compound **8** (a) or compound **20** (b, c). The crystallized **1** structure, **8**, or **20** are depicted in light blue, green, and purple sticks, respectively. The NMPRTase A and B chains are represented by gray sticks (a, b) and by molecular surface colored according to electrostatic potential. Positive potential is shown in blue, and negative potential is in red (c).

The three-dimensional model of the interactions between NMPRTase and **8** highlights its ability in reproducing the binding mode of **1** (Figure 15a). Except for the loss of the hydrogen bond with the water molecule common to all the triazole derivatives, the other pharmacophoric interactions are maintained: π stacking of the pyridine ring with Phe193 and Tyr18′, cation$-\pi$ with Arg196, and hydrogen bonds with the hydroxyl of Ser275. The biphenyl group on **8** remarkably contributes to the stability of the drug−target complex ($K_{\mathrm{dcalcd}\mathbf{8}} = 4.31 \times 10^{-9}$ M) occupying a shallow groove on the NMPRTase surface formed by Gly185, Tyr188, and Lys189 and interacting with Ile378, Ala379, Val399, and Arg349. The alkyl chain interacts with His191, Val242, Ile35′, and Arg31. In our calculated model, analogue **20** presents a binding mode very similar to that of **1** (Figure 15b), maintaining the interaction with the Phe193 and Tyr18′ aromatic ring and the hydrogen bond with the OH of Ser275. Additionally, the loss of the cation$-\pi$ interaction of the pyridine ring with Arg196 is balanced by the presence of the carbazole, which gives a cation$-\pi$ interaction with Lys89 and π stacking with Tyr188 ($K_{\mathrm{dcalcd}\mathbf{20}} = 3.07 \times 10^{-9}$ M). Moreover, such a rigid group allows better hydrophobic interactions with Glu376, Asn377, Arg349, Lys189, Ala379, and Ile378, and a part of it places on the shallow groove on the enzyme surface (Figure 15c) (Gly185, Tyr188, and Lys189). Our docking calculations would therefore suggest that the triazole ring, the pyridine ring, and the hydrophobic tail are related to hydrogen bonds, hydrophobic interactions, and aromatic stacking that constitute the driving forces of the target−ligand complexes. Molecular docking calculations also suggest that the triazole group must be linked directly to the pyridine ring, as confirmed by the loss of activity of **3** and that the hydrophobic tail can be increased for a wider interaction with the amino acids on the target surface, as observed for **8** and **20**. Obviously, such speculations will require further analogues to be synthesized and tested to verify this hypothesis.

Conclusions

In the present report, we have shown that click chemistry is applicable to the drug optimization process to generate structure−activity relationships. Following this strategy, we provide evidence that compound **8**, which presents a 2-aminobiphenyl aromatic group, is an inhibitor of NMPRTase. Although enzymatic assays have not been performed, biological data suggest that **8** shares the mechanism of action of **1**. The main observations that lead to this statement are as follows: (1) both **1** and **8** deplete NAD levels and are cytotoxic at similar concentrations; (2) both **1** and **8** induce autophagy; (3) the cytotoxic effects of **1** and **8** can be rescued by extracellular NAD application but cannot be rescued by nicotinamide. The metabolic instability of the pyridine moiety is one of the main problems of the two known inhibitors of NMPRTase in clinical trials (**1** and **2**), which leads to the need for continuous infusion.[31] On the basis of our data and structure−activity relationships, we believe that our

approach might lead to better modifications of the pyridine ring, affording more potent yet stable compounds.

Acknowledgment. Financial support from Regione Piemonte (Ricerca Sanitaria Finalizzata 2009 to G.C.T.) and MiUR (PRIN contract number 2006031151_005 to G.B.) is gratefully acknowledged. We dedicate this paper to Prof. Aldo Martelli on the occasion of his retirement.

Supporting Information Available: Biological and chemical experimental details, spectroscopic characterization (MS, IR, ^{1}H and ^{13}C NMR data) and elemental analysis of all the target compounds, viability data for all 185 compounds in the original screening, and molecular docking details. This material is available free of charge via the Internet at http://pubs.acs.org.

References

(1) Khan, J. A.; Forouhar, F.; Tao, X.; Tong, L. Nicotinamide adenine dinucleotide metabolism as an attractive target for drug discovery. *Expert Opin. Ther. Targets* **2007**, *11*, 695–705.
(2) Denu, J. M. The Sir 2 family of protein deacetylases. *Curr. Opin. Chem. Biol.* **2005**, *9*, 431–440.
(3) Belenky, P.; Bogan, K. L.; Brenner, C. NAD$^+$ metabolism in health and disease. *Trends Biochem. Sci.* **2007**, *32*, 12–19.
(4) Berger, F.; Ramírez-Hernández, M. H.; Ziegler, M. The new life of a centenarian: signalling functions of NAD(P). *Trends Biochem. Sci.* **2004**, *29*, 111–118.
(5) Genazzani, A. A.; Billington, R. A. NAADP: an atypical Ca^{2+}-release messenger? *Trends Pharmacol. Sci.* **2002**, *23*, 165–167.
(6) Malavasi, F.; Deaglio, S.; Funaro, A.; Ferrero, E.; Horenstein, A. L.; Ortolan, E.; Vaisitti, T.; Aydin, S. Evolution and function of the ADP ribosyl cyclase/CD38 gene family in physiology and pathology. *Physiol. Rev.* **2008**, *88*, 841–886.
(7) Magni, G.; Amici, A.; Emanuelli, M.; Orsomando, G.; Raffaelli, N.; Ruggieri, S. Enzymology of NAD$^+$ homeostasis in man. *Cell. Mol. Life Sci.* **2004**, *61*, 19–34.
(8) Bieganowski, P.; Brenner, C. Discoveries of nicotinamide riboside as a nutrient and conserved NRK genes establish a preiss-handler independent route to NAD$^+$ in fungi and humans. *Cell* **2004**, *117*, 495–502.
(9) Hasmann, M.; Schemainda, I. FK866, a highly specific noncompetitive inhibitor of nicotinamide phosphoribosyltransferase, represents a novel mechanism for induction of tumor cell apoptosis. *Cancer Res.* **2003**, *63*, 7436–7442.
(10) Nahimana, A.; Attinger, A.; Aubry, D.; Greaney, P.; Ireson, C.; Thougaard, A. V.; Tjørnelund, J.; Dawson, K. M.; Dupuis, M.; Duchosal, M A. The NAD biosynthesis inhibitor APO866 has potent antitumor activity against hematologic malignancies. *Blood* **2009**, *113*, 3276–3286.
(11) http://www.clinicaltrials.gov/ct2/results?term = APO866; accessed on May 25, **2009**.
(12) http://www.clinicaltrials.gov/ct2/results?term = GMX1777; accessed on May 25, **2009**.
(13) Schou, C.; Ottosen, E. R.; Petersen, H. J.; Björkling, F.; Latini, S.; Hjarnaa, P. V.; Bramm, E.; Binderup, L. Novel cyanoguanidines with potent oral antitumour activity. *Bioorg. Med. Chem.* **1997**, *7*, 3095–3100.
(14) Olesen, U. H.; Christensen, M. K.; Björkling, F.; Jäättelä, M.; Jensen, P. B.; Sehested, M.; Nielsen, S. J. Anticancer agent CHS-828 inhibits cellular synthesis of NAD. *Biochem. Biophys. Res. Commun.* **2008**, *367*, 799–804.
(15) Galli, U.; Ercolano, E.; Carraro, L.; Blasi Roman, C. R.; Sorba, G.; Canonico, P. L.; Genazzani, A. A.; Tron, G. C.; Billington, R. A. Synthesis and biological evaluation of isosteric analogues of FK866, an inhibitor of NAD salvage. *ChemMedChem* **2008**, *3*, 771–779.
(16) Khan, J. A.; Tao, X.; Tong, L. Molecular basis for the inhibition of human NMPRTase, a novel target for anticancer agents. *Nat. Struct. Mol. Biol.* **2006**, *13*, 582–588.
(17) Morris, G. M.; Goodsell, D. S.; Halliday, R. S.; Huey, R.; Hart, W. E.; Belew, R. K.; Olson, A. J. Automated docking using a Lamarckian genetic algorithm and empirical binding free energy function. *J. Comput. Chem.* **1998**, *19*, 1639–1662.
(18) (a) Kolb, H. C.; Finn, M. G.; Sharpless, K. B. Click chemistry: diverse chemical function from a few good reactions. *Angew. Chem., Int. Ed. Engl.* **2001**, *40*, 2004–2021. (b) Tornøe, C. W.; Christensen, C.; Meldal, M. Peptidotriazoles on solid phase: [1,2,3]-triazoles by regiospecific copper(I)-catalyzed 1,3-dipolar cycloadditions of terminal alkynes to azides. *J. Org. Chem.* **2002**, *67*, 3057–3064. (c) Rostovtsev, V. V.; Green, L. G.; Fokin, V. V.; Sharpless, K. B. A stepwise Huisgen cycloaddition process: copper(I)-catalyzed regioselective "ligation" of azides and terminal alkynes. *Angew. Chem., Int. Ed.* **2002**, *41*, 2596–2599.
(19) For medicinal chemistry applications of click chemistry see: (a) Kolb, H. C.; Sharpless, K. B. The growing impact of click chemistry on drug discovery. *Drug Discovery Today* **2003**, *8*, 1128–1137. (b) Tron, G. C.; Pirali, T.; Billington, R. A.; Canonico, P. L.; Sorba, G.; Genazzani, A. A. Click chemistry reactions in medicinal chemistry: applications of the 1,3-dipolar cycloaddition between azides and alkynes. *Med. Res. Rev.* **2008**, *28*, 278–308.
(20) Pagliai, F.; Pirali, T.; Del Grosso, E.; Di Brisco, R.; Tron, G. C.; Sorba, G.; Genazzani, A. A. Rapid synthesis of triazole-modified resveratrol analogues via click chemistry. *J. Med. Chem.* **2006**, *49*, 467–470.
(21) Pirali, T.; Gatti, S.; Di Brisco, R.; Tacchi, S.; Zaninetti, R.; Brunelli, E.; Massarotti, A.; Sorba, G.; Canonico, P. L.; Moro, L.; Genazzani, A. A.; Tron, G. C.; Billington, R. A. Estrogenic analogues synthesized via click chemistry. *ChemMedChem* **2007**, *2*, 437–440.
(22) (a) Pirali, T.; Pagliai, F.; Mercurio, C.; Boggio, R.; Canonico, P. L.; Sorba, G.; Tron, G. C.; Genazzani, A. A. Triazole-modified histone deacetylase inhibitors as a rapid route to drug discovery. *J. Comb. Chem.* **2008**, *10*, 624–627. (b) Brik, A.; Muldoon, J.; Lin, Y.; Elder, J. H.; Goodsell, D. S.; Olson, A. J.; Fokin, V. V.; Sharpless, K. B.; Wong, C. Rapid diversity-oriented synthesis in microtiter plates for in situ screening of HIV protease inhibitors. *ChemBioChem* **2003**, *4*, 1246–1248. (c) Lee, L. V.; Mitchell, M. L.; Huang, S.; Fokin, V. V.; Sharpless, K. B.; Wong, C. A Potent and high selective inhibitor of human α-1,3-fucosyltransferase via click chemistry. *J. Am. Chem. Soc.* **2003**, *125*, 9588–9589.
(23) L'Abbè, G.; Beenaerts, L. Influence of electron-withdrawing N-1 substituents on the thermal behavior of 5-azido-1,2,3-triazoles. *Tetrahedron* **1989**, *45*, 749–756.
(24) Pizzotti, M.; Cenini, S.; Porta, F. Reactions of 2-azidopyridine and 1-pyridinio ylides with transition-metal complexes. *J. Chem. Soc., Dalton Trans.* **1978**, 1155–1160.
(25) Ohira, S. Methanolysis of dimethyl(1-diazo-2-oxopropyl)phosphonate. Generation of (diazomethyl) phosphonate and reaction with carbonyl compounds. *Synth. Commun.* **1989**, *19*, 561–564.
(26) Müller, S.; Liepold, B.; Roth, G. J.; Bestmann, H. J. An improved one-pot procedure for the synthesis of alkynes from aldehydes. *Synlett* **1996**, 521–522.
(27) Billington, R. A.; Travelli, C.; Ercolano, E.; Galli, U.; Roman, C. B.; Grolla, A. A.; Canonico, P. L.; Condorelli, F.; Genazzani, A. A. Characterization of NAD uptake in mammalian cells. *J. Biol. Chem.* **2008**, *283*, 6367–6374.
(28) Billington, R. A.; Genazzani, A. A.; Travelli, C.; Condorelli, F. NAD depletion by FK866 induces autophagy. *Autophagy* **2008**, *4*, 385–387.
(29) Klionsky, D. J. Autophagy: from phenomenology to molecular understanding in less than a decade. *Nat. Rev. Mol. Cell. Biol.* **2007**, *8*, 931–937.
(30) Klionsky, D. J.; Abeliovich, H.; Agostinis, P.; Agrawal, D. K.; Aliev, G.; Askew, D. S.; Baba, M.; Baehrecke, E. H.; Bahr, B. A.; Ballabio, A.; et al. Guidelines for the use and interpretation of assays for monitoring autophagy in higher eukaryotes. *Autophagy* **2008**, *4*, 151–175.
(31) Beauparlant, P.; Bédard, D.; Bernier, C.; Chan, H.; Gilbert, K.; Goulet, D.; Gratton, M. O.; Lavoie, M.; Roulston, A.; Turcotte, E.; Watson, M. Preclinical development of the nicotinamide phosphoribosyl transferase inhibitor prodrug GMX1777. *Anti-Cancer Drugs* **2009**, *20*, 346–354.